Static and Dynamic Slider Air Bearing Behavior in Heat Assisted Magnetic Recording under Thermal Flying Height Control and Laser System Induced Protrusion

Joanna Bechtel Dahl* and David B. Bogy

Computer Mechanics Laboratory, Department of Mechanical Engineering, University of California at Berkeley, Berkeley, CA 94720, USA

November 15, 2013

Abstract

The air bearing's response to regions of elevated temperature on its bounding surfaces (the slider and disk) may be an important consideration in the head-disk interface design of heat assisted magnetic recording (HAMR) systems. We implement the general non-isothermal molecular gas lubrication equation into an iterative static solver and dynamic air bearing solver to evaluate the effect of localized heating of the air bearing surface (ABS) due to the near-field transducer (NFT). The heat dissipating components in our simplified HAMR design are the NFT, laser diode, and thermal flying height (TFC) control heater. We investigate the effect of each HAMR slider component on ABS temperature and thermal deformation and the slider's flying height. The NFT induces a localized thermal spot and protrusion on the larger TFC bulge, and it is the location of maximum temperature. This ABS temperature profile alters the air bearing pressure distribution, increasing the pressure at the hot NFT location compared to predictions of an isothermal air bearing solver, so that the center of the pressure acting on the ABS is slightly closer to the trailing edge, thereby decreasing the pitch angle and increasing the minimum flying height. Other researchers have shown the NFT's thermal response time may be much faster than it's protrusion response time [1]. The slider's dynamic response to a time-varying NFT thermal spot on the ABS while the combined TFC and NFT induced thermal protrusion remains constant is investigated with our dynamic air bearing solver. We simulate the slider's step response to a suddenly applied ABS temperature profile and a pulsed temperature profile that represents laser-on over data zones and laser-off over servo zones. The time-varying ABS temperature profile causes a time-varying pressure profile on the ABS. For the slider design and simulation conditions used here, the result of the pressure profile variation is to alter the x position of the center of pressure, thereby changing the pitch moment. In response, the pitch angle and minimum flying height change. The step response decays after approximately 0.15 ms. Because the laser duty cycle is much shorter than this response time, a periodic disturbance in the x coordinate, pitch angle, and minimum flying height is predicted. The peak-to-peak minimum flying height modulations are relatively small (only up to 0.126 nm); more significantly, the time-averaged minimum flying height increases 0.5 nm for the NFT that reached 208°C compared to simulations of the isothermal ABS at ambient temperature.

1 Introduction

The system developers in the hard disk drive industry generally agree that a new technology is needed to increase the storage density of hard disk drives (HDD) above 1 TB/in^2 and recapture the aggressive storage density annual growth rates of years past in order to meet the future digital data storage demand. Over the past few years, the industry has reached a consensus that heat assisted magnetic recording (HAMR) will be an early high density recording technology brought to market. Novel components such as a laser delivery system integrated into the slider and a new magnetic medium have been developed to the point

---

*Corresponding author: jobechtel@berkeley.edu

that a recent spin-stand recording demonstration of HAMR system technology claims to have achieved 1.007 Tb/in^2 [2]. However, the HAMR prototypes survive only a few write cycles [3], which is likely due to heating and structural damage of the plasmonic near-field transducer (NFT) [4]. Assuming a laser delivery system will be designed that does not exceed the damage threshold of the NFT, the temperature on the slider's air bearing surface (ABS) may still be several hundred degrees above ambient temperature. This laser delivery system will focus energy on the magnetic recording disk to a thermal spot with a full width at half maximum (FWHM) of 25 nm and maximum temperature around 500°C for > 1 TB/in^2 HAMR systems [5]. The air bearing's response to these regions of elevated temperature on its bounding surfaces may be an important consideration in head-disk interface (HDI) design.

Even though no production HAMR slider exists for research purposes outside the companies, a few experimental and simulation studies have been published that investigate thermal issues for sliders flying under HAMR conditions. Xu et al. [6] measured the effect of a pulsed laser on the slider's flying dynamics; the slider's vibration amplitude was about 0.2 nm for a 17.5-mW, 130–170 kHz pulsed laser. Comparing the results of a finite element simulation of the media subject to a heated area and a simple air bearing force calculation, they concluded that the thermal distortion of the disk surface is the main reason for the slider's flying height change. For these studies, the optically focused laser illuminated the lower side of the magnetic layer through the glass substrate, and the maximum media temperature was estimated to be 100°C. The laser delivery system was not integrated into the slider, and no NFT was present to confine the laser energy below the diffraction limit. Zheng et al. [7] used an iterative static solver to predict the thermal deformation and flying attitude of a sophisticated slider with dual thermal flying height control (TFC) heaters, read and writer elements, and two laser delivery system components, the waveguide and NFT. The dual heater design could compensate for waveguide-induced thermal protrusion if the power dissipated in the waveguide was less than the heater powers.

A series of papers from the Data Storage Institute investigated the impact of an integrated laser delivery system on the slider's thermal deformation, though not on the slider's flying performance. Xu et al. [8] present a thermo-mechanical analysis of a detailed integrated HAMR slider model that includes a laser diode, waveguide, coupling prism, and NFT as well as the suspension to which the slider is attached. However, in their model there is no TFC heater. The NFT temperature was predicted to be close to 250°C for the conditions simulated. In another study, Xu et al. [9] performed electromagnetic simulations and predicted a NFT efficiency of 2–3%. Other findings were that the NFT absorbed 10–25% of the incident energy from the waveguide and that the NFT temperature increased over 200°C when the distance between the write pole and NFT was reduced from 50 nm to 10 nm. The dynamic thermo-mechanical response of HAMR head components to a pulsed laser was investigated numerically in [1]. The authors found that the NFT protrusion does not follow the rapid temperature change of the pulsed laser. The NFT protrusion response time was 2–3 ms while the temperature response time was only 2 μs. The rest of the slider body demonstrated temperature response times of about 1 s.

All the previous studies mentioned above have focused on the details of thermal or electromagnetic energy transfer within the slider body and laser delivery system but not on the thermal effects on the air bearing. If the air bearing was included, either an isothermal air bearing solver designed for traditional non-HAMR sliders was used or the slider's flying attitude and pressure profile were assumed. Ambient temperature effects on the flying performance of non-HAMR sliders have been investigated numerically [10, 11]. However, a study of the thermal effects of localized ABS or disk heating on the air bearing static and dynamic performance has not been presented.

In earlier work, we implemented Fukui and Kaneko's non-isothermal molecular gas lubrication (MGL) equation [12] in an air bearing solver and performed static simulations on a production slider ABS rail design with approximate HAMR conditions [13]. For a prescribed Gaussian ABS temperature profile with a maximum temperature of 300°C and 160-μm FHWM (admittedly a large spot for a HAMR slider), the minimum flying height increased by over 1 nm when the ABS temperature profile was considered (3.49 nm) compared to an isothermal ABS at ambient temperature (2.42 nm). This preliminary study demonstrated that the non-isothermal MGL equation with a heated ABS can predict a significantly different slider flying attitude compared to the isothermal MGL equation. In the present paper we implement the non-isothermal MGL equation into a more accurate iterative static air bearing/slider thermo-mechanical solver and a dynamic air bearing solver.

First we describe a simplified HAMR slider model of our own design. We use the iterative static solver

employing the non-isothermal MGL equation to determine the slider's thermal deformation and temperature and resulting flying attitude for given heater power and NFT heat dissipation rates. The static results predicted by the isothermal and non-isothermal MGL equations are compared. Finally we present dynamic simulations that demonstrate the effect of a pulsed laser on the slider's flying dynamics.

2 Simplified HAMR Slider

Here we develop a simplified HAMR slider design with important laser delivery system components in addition to a thermally actuating heater to use for HAMR slider flying behavior analysis. We create a simple HAMR slider finite element model (Figure 1) loosely based on HGST's 'E-antenna' NFT design [14] and use an existing ABS rail design from a production TFC slider for the air bearing simulations (Figure 2). We ignore the read-write elements for simplicity in our analysis that concentrates on thermal effects, even though the write pole will interfere with the electromagnetic field in the nearby waveguide, absorbing some of electromagnetic energy that increases the write pole's temperature and adds to the slider's thermal deformation [15].

In order to work with a reasonable number of nodes, we do not include the etched ABS design in the finite element model; the etch depth dimensions (2.5 nm–1.6 μm) are small compared to most of the other mechanical dimensions of the slider. The thermal deformation determined by the finite element solver is merely added to the ABS etched design in the air bearing solver. The finite element model components are simply joined together with no interface thermal resistances. The displacements and temperatures of shared nodes are assumed to be equal.

We use bulk material properties for all the slider's components even though thin-film effects are likely important, especially around the NFT. The bulk of the slider is made of aluminum-titanium-carbon (AlTiC), a common substrate for air bearing sliders. The trailing edge portion of the slider with the embedded thermal fly height control heater is made of alumina (Al_2O_3) which is often used as an electrical insulator in integrated circuits. Nichrome (NiCr) is a high resistivity, non-magnetic alloy used for the TFC heater resistance wire that performs the electric heating. The NFT is made of gold (Au), a metal that supports surface plasmons. The diode is made of gallium arsenide (GaAs), a common semiconductor material use in near-infrared laser diodes. Tantalum pentoxide (Ta_2O_5) is used for the waveguide material due to its high refractive index contrast and low absorption properties that allow for strong confinement of light with low propagation losses; thin-film thermoelastic properties for Ta_2O_5 are used according to measurement from [16].

Table 1: HAMR slider component material properties. The properties are k thermal conductivity, α_T thermal expansion coefficient, E Young's modulus, ν Poisson's ratio, and ρ electrical resistivity.

Component	Material	k W/(m·K)	α_T K^{-1}	E GPa	ν –	ρ Ωm	Dimensions μm
Main Body	AlTiC	24.5	7.7e-6	390	0.24		$818.5 \times 700 \times 230$
TE Body	Al_2O_3	1.3	7.5e-6	200	0.23		$25 \times 700 \times 230$
Heater	NiCr	13.4	14e-6	165	0.3	1.0414e-6	$0.3 \times 4 \times 4$
NFT	Au	318	14.2e-6	79	0.44		$0.3 \times 0.6 \times 0.1$
Waveguide	Ta_2O_5	57.5	4.4e-6	136	0.27		$1 \times 1 \times 229.9$
Laser Diode	GaAs	33	5.7e-6	85.9	0.31		$600 \times 700 \times 150$

Figure 3 summarizes the light delivery pathway and regions of expected heat dissipation. Around 0.5 mW of energy is expected to be needed to heat a magnetic bit region of a FePt magnetic disk in HAMR writing [8]. Diodes generally convert about 50% of the input electrical power into electromagnetic wave energy (laser beam), and we assume that the remaining 50% is dissipated as heat in the diode. The overall optical efficiency from the exit of the laser diode to the entrance of the NFT is around 40% due to coupling losses [14]. The NFT is about 5% efficient, and it absorbs about 10–20% of the energy delivered by the waveguide [9]. The heat generations in the NFT and the diode are assumed to be uniformly distributed. The diode would likely be adhered to the back of the slider by some means, but we do not include a boundary thermal

resistance between the slider and disk or between any other slider components at this time. Analysis with Maxwell's equations shows that the magnetic write pole absorbs a 10–40% of the energy from the waveguide and dissipates that energy as heat [15]. However, for simplicity we are excluding the read and write elements for this study.

3   Molecular Gas Lubrication Equation for a HAMR Air Bearing

We use Fukui and Kaneko's [12] generalized Reynolds equation or molecular gas lubrication (MGL) equation that is derived from the linearized Boltzmann equation under the lubrication approximation. The non-dimensional MGL equation is

$$
\sigma \frac{\partial}{\partial \tau}\left(\frac{PH}{\overline{T}}\right) \quad + \quad \frac{\partial}{\partial X}\left[\Lambda_{x,0}\frac{PH}{\overline{T}} - \frac{PH^3}{\overline{\mu}\,\overline{T}}\overline{Q}_P\frac{\partial P}{\partial X} + \frac{P^2H^3}{\overline{\mu}\,\overline{T}^2}\overline{Q}_T\frac{\partial \overline{T}_w}{\partial X}\right]
$$
$$
+ \quad \frac{\partial}{\partial Y}\left[\Lambda_{y,0}\frac{PH}{\overline{T}} - \frac{PH^3}{\overline{\mu}\,\overline{T}}\overline{Q}_P\frac{\partial P}{\partial Y} + \frac{P^2H^3}{\overline{\mu}\,\overline{T}^2}\overline{Q}_T\frac{\partial \overline{T}_w}{\partial Y}\right] = 0 \qquad (1)
$$

where the non-dimensional squeeze number and bearing numbers in the x and y directions are defined as

$$
\sigma = \frac{12\mu_0\omega_0 L^2}{p_0 h_m^2} \tag{2a}
$$

$$
\Lambda_{x,0} = \frac{6LU\mu_0}{p_0 h_m^2} \tag{2b}
$$

$$
\Lambda_{y,0} = \frac{6LV\mu_0}{p_0 h_m^2} \tag{2c}
$$

The non-dimensional quantities are $X = x/L$, $Y = y/L$, $Z = z/h_m$, $H = h/h_m$, $P = p/p_0$, $\overline{\mu} = \mu/\mu_0$, $\overline{T} = T/T_0$, and $\tau = \omega_0 t$. The subscript '0' denotes ambient conditions. Here $\overline{T}$ is local air temperature and τ is time. L is the characteristic lubrication region length, the slider length in the case of an air bearing simulation. h_m is a reference clearance at the slider's trailing edge center (TEC). P is the air bearing pressure, and $\overline{\mu}$ is the air viscosity. U and V are the planar direction disk speeds from the perspective of the slider as determined from the skew angle. $\Lambda_{x,0}$, $\Lambda_{y,0}$ are system parameters, constant for a particular head-disk system with a constant rotational speed because they depend on ambient properties. X corresponds to the slider's length direction (down-track), Y corresponds to the slider's width direction (cross-track), and Z is the air bearing thickness direction. $\partial\overline{T}_w/\partial X$, $\partial\overline{T}_w/\partial Y$ are the boundary wall temperature gradients, i.e. the ABS and disk temperature gradients. ω_0 is a characteristic angular frequency equivalent to the disk rotational speed. $\overline{Q}_P$, and $\overline{Q}_T$ are the relative non-dimensional flow rates for Poiseuille, and thermal creep flow determined from kinetic theory [17, 18]. These flow rates depend on the local Knudsen number, $\text{Kn} = \lambda/h$.

For non-isothermal systems in which the fluid temperature is unknown, the energy equation must also be solved simultaneously. However, in this work we simplify our analysis by assuming we know the air temperature so as to bypass solving the energy equation. As a first approximation, the temperature of the air at a particular point (x,y) is estimated to be the average of the disk and slider temperature at that point.

The conventional air bearing solvers that evaluate non-HAMR sliders use the MGL equation that is simplified for isothermal conditions in which $\overline{T} = \overline{\mu} = 1$ and $\partial\overline{T}_w/\partial X = \partial\overline{T}_w/\partial Y = 0$:

$$
\sigma\frac{\partial(PH)}{\partial\tau} + \frac{\partial}{\partial X}\left(\Lambda_x PH - PH^3\overline{Q}_P\frac{\partial P}{\partial X}\right) + \frac{\partial}{\partial Y}\left(\Lambda_y PH - PH^3\overline{Q}_P\frac{\partial P}{\partial Y}\right) = 0 \qquad (3)
$$

Equation 3 can be interpreted as a convection-diffusion equation in which the quantity PH is convected through the air bearing by a non-dimensional fluid velocity Λ. For the non-isothermal MGL equation (Equation 1), the convected quantity is $PH/\overline{T}$.

In order to solve the governing equation of the air bearing, we need to know the local air viscosity and mean free path. Mean free path depends on local pressure and temperature according to the hard sphere model and the ideal gas law [19]. Therefore, in the air bearing of a hard disk drive, the mean free path of the

air molecules is assumed to be proportional to the local temperature and inversely proportional to the local pressure: $\lambda/\lambda_0 = T/T_0 \cdot p_0/p$. The air viscosity, a function of temperature, is calculated using Sutherland's Formula for the viscosity of a gas that treats air molecules as hard spheres with a weak attractive force [19, 20].

We consider conductive heat transfer from the air bearing surface in the thermo-mechanical model of the slider. An expression for the conductive heat flux at the ABS was first presented by Zhang et al. [21] and later improved by Chen et al. [22] to account for the close proximity of two bounding surfaces on the mean free path.

4 Numerical Air Bearing Solver

The Computer Mechanics Laboratory at the University of California, Berkeley has developed an air bearing solver, CMLAir, to solve the isothermal MGL equation [23–25]. The static version determines the air bearing pressure profile that balances the applied suspension load (vertical suspension force and pitch and roll moments) and other HDI forces: asperity contact force, intermolecular force and electrostatic force. The asperity contact force due to the roughness of the contacting surfaces is implemented in CMLAir using the Greenwood-Williamson asperity contact model [26–28]. The intermolecular force between the slider and the disk is based on the Lennard-Jones potential [29]. The electrostatic force in the HDI arises from the tribocharging phenomena [30]. The dynamic solver simultaneously solves the transient MGL equation and the equations of motion for the slider-suspension assembly to determine the air bearing pressure distribution that balances the applied suspension load, HDI forces, and slider inertia at each time step. For this study, we modify the governing equation of CMLAir from the isothermal MGL equation (Equation 3) to the general non-isothermal equation (Equation 1). We denote this new air bearing solver as CMLAir-HAMR.

The static flying attitude and thermal deformation solutions of a TFC slider or HAMR slider must be solved by an iterative approach. The air bearing and slider's thermal deformation solutions are related to each other through boundary conditions at the ABS (heat transfer coefficient and pressure, temperature and protrusion). The air bearing solver predicts the air bearing pressure profile and flying attitude of a slider for a given suspension load, slider thermal protrusion profile, and now the ABS temperature profile, a new feature for CMLAir-HAMR. The thermal protrusion due to specified heat generating components can be determined from a finite element solver such as ANSYS where the heat transfer boundary conditions and the pressure force at the air bearing surface depend on the slider's flying attitude and pressure profile. An iterative solver between the commercial finite element software ANSYS and the static version of CMLAir-HAMR is developed, based on the CML TFC code [31]. The user specifies the TFC heater power and the amount of heat dissipated in the laser delivery system components. The iterations between ANSYS and CMLAir-HAMR continue until the flying height obtained from two consecutive iterations is within a specified tolerance (0.05 nm).

For the dynamic air bearing solver, the computation time required to iterate with a finite element solver at each time step would be prohibitively expensive. Therefore the ABS temperature and thermal protrusion profiles determined for a particular TFC heater power and NFT dissipation rate serve as realistic and accurate starting base profiles to be interpolated for the dynamic simulation. The peak ABS temperature and thermal protrusion values are specified at each time. The temperature and protrusion over the entire ABS are determined by scaling the base profiles according to specified peak values to realize sharpening peak profiles.

5 Iterative Static Solver Results

5.1 HAMR Slider Component Effect Study

In the process of developing our HAMR slider, we added components one-by-one and tested the impact of the additional components on the predictions of the iterative static solver. The components were added in the following order: TFC heater, NFT, waveguide, and laser diode. The static simulations occur at a disk radial position of 22.215 mm with a skew angle of 0.953 degrees. The disk is spinning at 5400 RPM. The 2.5 g-force suspension load is applied at the slider's geometric center (no offset). The suspension has a preloaded 0.74-μN·m static pitch torque and 0-μN·m static roll torque. The intermolecular force constants are $A = 10^{-19}$ J

(Hamaker constant) and $B = 10^{-26}$ J·m. The disk is assumed to have a roughness represented by an asperity distribution with a number density of 212.42 μm^{-2}, standard deviation in asperity height of 0.87 nm, and mean radius of curvature of 0.43 μm. For the asperity contact modeling, the disk material properties are Young's modulus of 111.59 GPa, yield strength of 1000 GPa, Poisson's ration of 0.3, and friction coefficient of 0.3. The electrostatic force is not included.

The following boundary conditions are used in the iterative static solver. Displacement boundary conditions are applied to the slider to approximate the attachment to the suspension system, thereby transmitting the suspension load. The laser diode is attached to the back of the slider, and on the back of the diode (farthest face from the ABS) the displacement is constrained to be fixed in the vertical z direction. The two corners at the leading edge are fixed. We are not including the suspension in this model because it adds complexity that we deem unnecessary to perform early-stage thermo-mechanical analyses of the HAMR thermal effects on the air bearing. Convective boundary conditions are defined on each external face of the slider finite element model. At a rotational speed of 5400 RPM, boundary layer theory predicts the convection coefficient on the non-ABS faces of the slider is on the order of 100 W/(m^2·K) [32]. We use a higher convective heat transfer coefficient of 2000 W/(m^2·K) on the top of the slider to approximate the heat-carrying capacity of the metal suspension. On the air bearing surface, we use the film coefficient derived from slip theory [21, 22].

Figure 4 presents the minimum flying heights at various heater powers for four different sliders with varying amounts of laser delivery system components. The minimum flying height is determined by slider type. The heater-only slider corresponds to a conventional TFC slider currently used in HDD products, and it has the highest flying height at all heater power levels. The presence of the heat-generating NFT results in lower flying heights. The slider with the lowest flying height is the slider with only the heater and NFT. There is not much difference in the minimum flying heights between the final two sliders that only differ by the presence of the laser diode on the backside of the slider. The minimum flying heights of the three sliders containing a NFT converge at around 25 mW when the flying height drops below 2 nm.

The inclusion of HAMR laser delivery system components affects the heat transfer within the slider's body and from the ABS, resulting in different ABS temperatures and thermal protrusion profiles that are the reason for the differences in the minimum flying heights predicted by the air bearing solver. The ABS temperatures and protrusion profiles determined by the finite element solver for the case of 27-mW heater power are plotted in Figure 5. All slider types have a similar ABS temperature profile away from the NFT region, as seen in Figure 5a. The TFC slider (heater-only) has a low temperature, around 40°C, in the trailing edge region. The localized sharp temperature spike at the NFT location is due to the insulating feature of the surrounding alumina that keeps much of the dissipated heat at the NFT. The lower temperature on the leading edge side of the NFT is an artifact of the quadratic interpolation of ABS temperature imported from the finite element solver; these interpolation issues were later fixed by using a finer grid within the air bearing solver. This artificial drop in temperature is small enough so that the simulation results are not appreciably affected. For sliders containing a waveguide adjacent to the back of the NFT, the temperature at the NFT is approximately 50°C lower than the slider without the waveguide. This is due to relatively high thermal conductivity of the waveguide; with $k = 57.5$ W/(m·K), the Ta$_2$O$_5$ waveguide conducts heat generated by the NFT away from the ABS more efficiently than the electrically insulating alumina with $k = 1.3$ W/(m·K).

The NFT protrudes from the surrounding material, creating a relatively sharp protrusion point shown in Figure 5b for sliders that include the NFT. This is a result of the gold NFT having a thermal expansion coefficient roughly twice that of alumina and three times that of the waveguide and the NFT being the location of maximum temperature and therefore maximum thermal expansion. The large temperature spike for the heater-NFT-only slider results in the sharpest protrusion profile at the NFT location. The presence of the 50-mW dissipating diode does not significantly affect the temperature profile or protrusion profile. The diode's minor effect is to slightly increase the amount of thermal protrusion compared with the slider containing the NFT and waveguide. The sharp change in ABS protrusion at 818 μm is due to the change in etch depth from 0 nm to 2.54 nm (recall Figure 2). In Figure 6, the flying height along the slider's centerline near the trailing edge is detailed for the case of 27-mW heater power. The flying height profile closely mirrors the protrusion profile, indicating the thermal protrusion of the slider is an important factor for determining the flying height.

5.2 Air Bearing Solver Governing Equation Study

We are interested in the difference in the slider's flying attitude as predicted by the air bearing solver based on the non-isothermal MGL Equation 1 (CMLAir-HAMR) and the isothermal MGL Equation 3 (CMLAir) for our HAMR slider. Iterative static simulations are performed for two cases that differ only in the ABS temperature. For the 'non-isothermal ABS' case, the ABS temperature and protrusion determined by the finite element solver are used as boundary conditions in the air bearing solver. For the 'isothermal ABS' case, only the thermally induced protrusion determined by ANSYS is used as an air bearing boundary condition; the ABS is specified to be isothermal at ambient temperature (25°C) within the air bearing solver so that the solver finds the solution to the isothermal MGL equation.

In order to isolate ABS temperature effects on the air bearing, we neglect the intermolecular and contact forces. So the only pressure exerted on the ABS is due to the air bearing. The rest of the simulation conditions, except heater power and NFT dissipation rates, are the same as Section 5.1.

Figure 7 presents the ABS temperature and protrusion profiles predicted by the finite element solver that are used as boundary conditions in the air bearing solver. Figure 7a depicts the centerline ABS temperature profiles for both cases. The ABS temperature is prescribed to be 25°C for the isothermal ABS case. For the non-isothermal ABS case, the thermal spot due to the NFT has a maximum temperature of 285°C and its size is approximately 3.6 μm FWHM. The ABS thermal protrusion is practically the same for both cases as shown in Figure 7b. The abrupt changes in the ABS protrusion are due to the rail design.

The simulation results for 'non-isothermal' vs. 'isothermal' ABS cases are presented in Table 2 and Figures 8–9. Compared with the isothermal ABS case, the non-isothermal ABS case has a slightly lower pitch angle that leads to a higher minimum flying height by approximately 0.2 nm (Table 2). The roll angle is not appreciably affected.

Table 2: Iterative static solver flying attitude results for the cases of a non-isothermal ABS determined by the finite element solver and a prescribed isothermal ABS.

	Pitch Angle μrad	Roll Angle μrad	Minimum Flying Height nm
Isothermal ABS	81.12	2.365	1.63
Non-isothermal ABS	80.72	2.428	1.86

Comparing Equations 1 and 3, one can expect that for a given bounding geometry H, the air bearing pressure distribution P needed to everywhere satisfy Equation 1 is different from the pressure distribution that everywhere satisfies Equation 3 due to the presence of $\overline{T}$ and $\overline{\mu}$ in that equation that vary within the domain. The ABS protrusion is shown to be effectively the same for the two cases (Figure 7b), so the higher air bearing pressure prediction for the non-isothermal ABS case (Figure 8) is due to the consideration of the hot spot at the NFT. The peak pressure at the NFT is 4.29 MPa for the non-isothermal ABS and 3.65 MPa for the isothermal ABS.

The slider's pitch angle depends on the balance of moments of pressure on the leading and trailing portions of the ABS. The non-isothermal ABS has a higher pressure at the NFT, near the trailing edge, so the center of pressure is closer to the trailing edge compared to the isothermal ABS case. This changes the pitch moment of the slider so that the pitch angle is lower and minimum flying height at the trailing edge is slightly higher, as shown in Figure 9a. The difference in minimum flying height along the full length of the slider at its centerline is given in Figure 9b. The difference increases linearly from -0.1 nm at the leading edge to 0.23 nm at the trailing edge. This is a result of the decrease in pitch angle when the ABS temperature is considered in the air bearing solver.

Because the skew angle is close to zero, the ABS design is almost symmetric, and the temperature and protrusion profiles are nearly symmetric, the pressure distribution is also approximately symmetric across the slider's centerline for both cases. Thus the balance of the moments of pressure on the left and right sides of the slider are approximately equal so the roll angle is small.

7

6 Dynamic Simulation Results

Experiments have revealed that localized heating of the disk by a pulsed laser leads to flying height modulations [6], and simulations predict that the NFT temperature response time is rapid (2 μs) while the thermal protrusion response is much slower (2–3 ms) [1]. With our dynamic solver, we can test if rapid fluctuations in NFT temperature alone can affect the slider's flying attitude while the protrusion remains constant. Here we consider only thermal effects due to the hot NFT on the ABS; the disk is assumed to be smooth and isothermal at ambient 25°C.

Two sets of dynamics simulations are presented. The first set is the step response of the air bearing and the slider's flying attitude due to a sudden change in the ABS temperature profile. Five ABS temperature profiles are considered: an isothermal 25°C profile and four temperature profiles with maximum temperature of 74°C, 119°C, 163°C, and 208°C. These profiles correspond to increases in maximum temperature of 0°C, 49°C, 94°C, 138°C, and 183°C. The second set of simulations replicate a pulsed laser that is in the on-state when flying over data zones and in the off-state over server zones. For a disk spinning at 5400 RPM and assuming there are 250 servo sectors that comprise 6% of the track, the laser duty cycle is 41.778 μs on-time and 2.6667 μs off-time. A 2-μs response time is incorporated into the prescribed ABS peak temperature jumps so that the NFT temperature response is more realistic.

Simulations are run for a total of 1 ms. The base profiles for the ABS temperature and protrusion are from the 24-mW TFC heater, 2-mW NFT iterative static solver result. The ABS thermal protrusion is prescribed to have a constant peak protrusion of 16.56 nm throughout the entire simulation, i.e. the ABS protrusion does not vary in time. The ABS temperature profile is either suddenly increased or pulsed, as described above. For the step response simulations, the ABS temperature profile increase is applied at 0.5 ms. The following dynamic simulations occur at a disk radial position of 22.215 mm with a skew angle of 0.953 degrees. The 2.5 g-force suspension load is applied at the slider's geometric center. Intermolecular forces between the slider and disk are included. The disk is assumed to be perfectly smooth, and there is no contact.

Table 3 contains the values of the center of pressure coordinates, pitch and roll angles, and minimum flying height after the step response of the slider's flying dynamics has settled and steady state is recovered. The center of pressure is for the total force acting on the ABS: the sum of the integrated air bearing pressure and intermolecular forces. For the conditions simulated here, the intermolecular force contribution to the total force acting on the ABS is much less than that of the air bearing: intermolecular forces contributes roughly -0.004 g-force while the air bearing applies 2.504 g-force to balance the 2.5 g-force suspension load. The center of pressure is not exactly on the slider's centerline ($y = 0$) because of the slight asymmetry of the ABS rail design and the non-zero skew angle. Both of the pressure center x and y coordinates change less than 1 nm except for the x coordinate in the ABS maximum temperature $(\Delta T_s)_{max} = 183°$C case. The center of pressure is a reflection of the balance of pressure front-to-rear (x coordinate) and left-to-right (y coordinate). Even though the center of pressure is in a similar location for all ABS temperature profiles, the difference is enough to slightly lower the pitch angle as the x coordinate moves slightly towards the trailing edge in response to the hot NFT on the ABS. The decrease in pitch increases the minimum flying height as much as 0.48 nm. The roll angle is not affected as much as the pitch angle; however, the roll angle does not affect the minimum flying height to the same degree the pitch angle does.

The time history of center of pressure coordinates, pitch and roll angles, and minimum flying height for

Table 3: Steady state values following settling of the HAMR slider's step ABS temperature response.

$(\Delta T_s)_{max}$	Pressure Center x Coordinate	Pressure Center y Coordinate	Pitch Angle	Roll Angle	Minimum Flying Height
°C	μm	μm	μrad	μrad	nm
0	419.2878	0.0066	73.21	1.960	1.17
49	419.2887	0.0065	72.95	1.947	1.32
94	419.2887	0.0065	72.75	1.937	1.43
138	419.2887	0.0064	72.57	1.927	1.54
183	419.2895	0.0064	72.38	1.918	1.65

the step response and pulsed response are presented in Figures 10–14 for a 0.15 ms time window long after the initial transients settle within the first 0.2 ms. In each figure, the quantity of interest is plotted along with the prescribed maximum ABS temperature. In Figure 10a, the oscillating x coordinate requires approximately 0.15 ms to equilibrate to it's steady state value listed in the second column of Table 3. This settling time is longer than the laser duty cycle, so for the pulsed laser, the pressure distribution is repeatedly disturbed and the pressure center x coordinate oscillates back and forth along the slider length as much as 1.3 μm . The modulating center of pressure x coordinate means a modulating pitch moment, which affects the slider's pitch angle (Figure 11). For the pulsed laser case, the pitch angle oscillates around the steady state value from Table 3 with a peak-to-peak variation that increases with increasing $(\Delta T_s)_{max}$. The maximum peak-to-peak variation is 0.285 μrad for the hottest ABS case. The center of pressure y coordinate responses are plotted in Figure 12 using the same scale as the x coordinate responses in Figure 10. The variation in the y coordinate is small in comparison to the variation in the x coordinate. The result is a minor change in roll angle compared to the change in pitch angle (Figure 13).

The modulating pitch angle drives a modulating minimum flying height (Figure 14). As with the pitch angle response, the minimum flying height oscillates around the steady state value from Table 3 with a peak-to-peak variation of about 0.126 nm for the hottest ABS case. These simulations predict that the hot NFT alone can alter the slider's flying dynamics.

7 Discussion

The use of the non-isothermal MGL equation with a varying ABS temperature profile results in a different prediction for air bearing pressure distribution from that predicted by the isothermal MGL equation with the ABS at ambient temperature. The new pressure distribution alters the air bearing force moments, decreasing the pitch angle and increasing the minimum flying height in this particular study. The minimum flying height peak-to-peak variation in the pulsed laser dynamic simulations may not be significant; in the worst case, the minimum flying height oscillated 0.126 nm. Though a significant portion of a targeted 1-nm flying height, this amount of flying height modulation would be difficult to isolate and observe experimentally from all the thermo-mechanical issues of a HAMR slider. The small modulations in pitch angle and flying height could possibly be mitigated by designing the ABS so that the air bearing has a higher stiffness. However, the change in steady state minimum flying height, or for the pulsed laser the time-averaged minimum flying height, is predicted to increase almost 0.5 nm for our HAMR slider design when the nano-scale NFT is heated to 208°Ccompared with an isothermal ABS at 25°C. This amount of flying height change could be considered significant to HDI and air bearing engineers.

Our simulation results predict that dynamic slider ABS temperature profiles with constant geometry (both on the disk and slider) can cause slider flying height modulations. In [6], Xu et al. concluded that the thermal distortion of the disk was the main cause for flying height modulation in their experiments. In this paper, we do not exactly replicated their experiments in simulation. We use a HAMR slider with an integrated laser delivery system while the slider in [6] was likely a conventional slider. Our simulations occur at lower flying heights, less than 2 nm compared to 11 nm reported by Xu et al. The thermal spot on the ABS due to the NFT found in our simulations is larger and hotter than the thermal spot estimated on the media in their experiments: the ABS temperature profiles we report are approximately Gaussian with a FWHM of 3.6 μm and maximum temperature up to 208°C, while Xu et al. report a laser illumination spot of roughly 550 nm, which may or may not correspond to the thermal profile size, and a maximum disk temperature around 100°C. So we are not contradicting the explanation of the experimental observations in [6]. Rather we were inspired by their work to investigate if NFT temperatures plausible in HAMR systems could significantly alter air bearing performance.

Some of our simulation results are comparable to the thermo-mechanical modeling of an integrated HAMR slider performed by Xu et al. [8]. We use the same heat transfer model from the ABS and similar convective boundary conditions on the non-ABS slider faces. The slider finite element model in [8] is similar to ours except for their addition of two components we excluded (a prism coupling the laser from the diode to the waveguide and a suspension) and a defined boundary thermal resistance between the diode and slider representing a soldering joint. However, in [8] the air bearing problem is not solved; instead the finite element solver is used with a prescribed pressure profile and flying attitude. In reality, the air bearing

pressure increases with decreasing minimum flying height, and that increases the conductive heat transfer from the ABS according the model from [21, 22]. In [8], one figure shows only a 0.5°C decrease in the NFT temperature (gold, 1-mW heat dissipation rate) for a decrease in minimum flying height from 8 nm to 4 nm (the smallest flying height used). Our simulations predicted similar results for a comparable system: for the 1-mW NFT case, we predict a NFT temperature drop of 0.2°C for a decrease in minimum flying height from 7.4 nm to 3.2 nm. However the constant pressure assumed by Xu el al. [8] is not expected to give accurate NFT temperature results if the flying height is decreased below 4 nm. Xu et al. [8] predict an NFT temperature of 250°C for 1-mW NFT power and 475°C for 2-mW NFT power with a minimum flying height of 2 nm; we predict lower NFT temperatures for similar conditions: 184.5°C NFT temperature for 1-mW NFT power at 3.3-nm minimum flying height and 312.3°C for 2-mW NFT power at 3.8-nm minimum flying height. Our lower predicted NFT temperature is also due in part to our choice of waveguide material; we use a higher thermal conductivity waveguide material that can more easily conduct heat away from the NFT and cool it. They observed 2 nm of protrusion at the NFT location due to its higher temperature and larger co-efficient of thermal expansion. We show slightly less NFT protrusion compared to the surrounding material, closer to 0.6 nm under similar simulation conditions, because of our choice of the waveguide material that has a similar coefficient of thermal expansion as the NFT and also because of our lower NFT temperature.

If the temperature and thermal deformation of the disk is considered, the slider's flying height modulations and the time-averaged flying height value could be greater than in the dynamic simulation results presented here. The air bearing pressure is higher in the hot NFT region compared to isothermal conditions (Figure 8a), so we hypothesize that the additional hot disk region would also locally increase the air bearing pressure and could significantly increase the flying height if it is located under the slider's NFT region. Though the disk would be much hotter than the ABS with a maximum temperature 400–500°C, the peak temperature spot could be as small as 25-nm FHWM. This very small spot may not have time to influence the much larger slider due to its small size and the rapidly rotating disk. But if this thermal spot on the disk is located directly under the NFT, its effect on air bearing dynamics could be surprisingly large due to the larger implications of thermal effects at locations of smaller spacing.

The ANSYS analysis presented here uses macroscopic field theories in the coupled-field analysis: Maxwell's equations for the electrical analysis, Fourier's law for heat condition in the thermal analysis, and linear elasticity for the structural analysis. These theories employ a continuum assumption. For the tiny features of an integrated HAMR slider—the NFT is only 100 nm thick and 300–600 nm in lateral dimensions—continuum theory may need some modification. The HAMR slider heat transfer problem requires a different type of analysis that is not limited by continuum assumptions. The aim of this work is to gain insight into the performance of the air bearing under HAMR conditions. A more accurate finite element heat transfer analysis is left to other researchers. When and if reliable HAMR sliders are built and become available, they would provide a means to experimentally validate any nanoscale thermo-mechanical simulation tools that are developed.

We only tested one slider design in this work. The magnitude and possibly direction of displacement of the center of pressure, pitch, roll, and flying height variation are likely dependent on the ABS rail design. The particulars of NFT heat transfer are also slider-design dependent.

8   Conclusion

In this paper, we study air bearing performance under static and dynamic conditions for a simplified HAMR slider design using an air bearing solver based on the non-isothermal molecular gas lubrication equation. An iterative static solver is used to determine the equilibrium flying conditions and thermal deformation of a HAMR slider with a complicated ABS rail design. The components that dissipate heat are the TFC heater, NFT, and laser diode. The NFT induces localized protrusion and has the highest temperature. The Ta_2O_5 waveguide dissipates heat away from the NFT and lowers the ABS maximum temperature, leading to a relatively smooth NFT protrusion. The laser diode does not appreciably affect the slider's air bearing and thermo-mechanical state for this particular slider design. For a given ABS protrusion, the non-isothermal MGL equation predicts a higher pressure in the region surrounding the hot NFT compared to the predictions of the isothermal MGL equation. This leads to a center of pressure that is slightly closer to the trailing edge, which decreases the pitch angle and therefore increases the minimum flying height. The effect on the roll angle is negligible in comparison to the pitch angle due to the near-zero skew angle and nearly symmetric

ABS design, temperature, and protrusion.

Dynamic air bearing simulations are conducted for step and pulsed ABS temperature profiles while the ABS protrusion profile remains constant. The time-varying ABS temperature profile induces a time-varying pressure profile. The x coordinate of the pressure center is appreciably affected, thereby altering the pitch angle and minimum flying height. The step response decays after approximately 0.15 ms. Because the laser duty cycle is much shorter than this response time, a periodic disturbance in the x coordinate, pitch angle, and minimum flying height results. For the ABS design and simulation conditions studied here, the peak-to-peak minimum flying height modulations are relatively small (only up to 0.126 nm); more significantly, the time-averaged minimum flying height increased 0.5 nm for the simulation with the NFT that reached $208°C$ compared to the simulation with the $25°C$ isothermal air bearing case.

Acknowledgements

References

[1] B Xu, J Li, Y Toh, K Ye, and J Zhang, "Dynamic Thermal Responses of Heat-Assisted Magnetic Recording Head in Data Writing Process," *IEEE Transactions on Magnetics*, vol. 48, no. 11, pp. 3280–3283, 2012.

[2] A. Q. Wu, Y. Kubota, T. Klemmer, T. Rausch, C. Peng, Y. Peng, D. Karns, X. Zhu, Y. Ding, E. K. Chang, Y. Zhao, H. Zhou, K. Gao, J.-U. Thiele, M. Seigler, G. Ju, and E. Gage, "HAMR Areal Density Demonstration of 1+ Tbpsi on Spinstand," in *The Magnetic Recording Conference (TMRC) 2012*, San Jose, CA, USA, 2012.

[3] W. Challener, C. Peng, A. Itagi, D. Karns, W. Peng, Y. Peng, X. Yang, X. Zhu, N. Gokemeijer, Y.-T. Hsia, G. Ju, R. Rottmayer, and M. Seigler, "Heat-assisted magnetic recording by a near-field transducer with efficient optical energy transfer," *Nature Photonics*, vol. 3, pp. 220–224, 2009.

[4] B. V. Budaev and D. B. Bogy, "On the lifetime of plasmonic transducers in heat assisted magnetic recording," *Journal of Applied Physics*, vol. 112, no. 3, p. 034 512, 2012.

[5] M. Kryder, E. Gage, T. McDaniel, W. Challener, R. Rottmayer, G. Ju, Y.-T. Hsia, and M. Erden, "Heat Assisted Magnetic Recording," *Proceedings of the IEEE*, vol. 96, no. 11, pp. 1810–1835, 2008.

[6] B. Xu, H. Yuan, J. Zhang, J. Yang, R. Ji, and T. Chong, "Thermal effect on slider flight height in heat assisted magnetic recording," *Journal of Applied Physics*, vol. 103, no. 7, 07F525, 2008.

[7] H. Zheng, H. Li, and F. E. Talke, "Numerical simulation of thermal flying height control sliders in heat-assisted magnetic recording," *Microsystem Technologies*, vol. 18, no. 9-10, pp. 1731–1739, 2012.

[8] B. Xu, C. W. Chia, Q. Zhang, Y. T. Toh, C. An, and G. Vienne, "Thermal Analysis of Heat-Assisted Magnetic Recording Optical Head with Laser Diode on Slider," *Japanese Journal of Applied Physics*, vol. 50, no. 9, 09MA05, Sep. 2011.

[9] B Xu, Y Toh, C Chia, J Li, J Zhang, K. Ye, and C. An, "Relationship between near field optical transducer laser absorption and its efficiency," *IEEE Transactions on Magnetics*, vol. 48, no. 5, pp. 1789–1793, 2012.

[10] N. Liu and D. B. Bogy, "Temperature Effect on a HDD Slider's Flying Performance at Steady State," *Tribology Letters*, vol. 35, no. 2, pp. 105–112, 2009.

[11] W. D. Zhou, C. H. Wong, B. Liu, S. K. Yu, and W Hua, "Effects of temperature dependent air properties on the performances of a thermal actuated slider," *Tribology International*, vol. 42, no. 6, pp. 902–910, 2009.

[12] S. Fukui and R. Kaneko, "Analysis of ultra-thin gas film lubrication based on linearized Boltzmann equation: First report derivation of a generalized lubrication equation including thermal creep flow," *ASME Journal of Tribology*, vol. 110, pp. 253–262, 1988.

[13] J. E. Bechtel and D. B. Bogy, "Heat-Assisted Magnetic Recording Air Bearing Simulations That Account for Lateral Air Temperature Variation," *IEEE Transactions on Magnetics*, vol. 47, no. 10, pp. 2379–2382, 2011.

[14] B. C. Stipe, T. C. Strand, C. C. Poon, H. Balamane, T. D. Boone, J. A. Katine, J.-L. Li, V. Rawat, H. Nemoto, A. Hirotsune, O. Hellwig, R. Ruiz, E. Dobisz, D. S. Kercher, N. Robertson, T. R. Albrecht, and B. D. Terris, "Magnetic recording at 1.5 Pb m^{-2} using an integrated plasmonic antenna," *Nature Photonics*, vol. 4, no. 7, pp. 484–488, 2010.

[15] M. Seigler, W. A. Challener, E Gage, N Gokemeijer, G Ju, B Lu, K Pelhos, C Peng, R. Rottmayer, and X Yang, "Integrated heat assisted magnetic recording head: Design and recording demonstration," *IEEE Transactions on Magnetics*, vol. 44, no. 1, pp. 119–124, 2008.

[16] E. Cetinorgu, B. Baloulas, O. Zabeida, J. Klemberg-Sapieha, and L. Martinu, "Mechanical and thermoelastic characteristics of optical thin films deposited by dual ion beam sputtering," *Applied Optics*, vol. 48, no. 23, pp. 4536–4544, 2009.

[17] C. Cercignani, M. Lampis, and S. Lorenzani, "Flow of a rarefied gas between parallel and almost parallel plates," in *Proceedings of 24th International Symposium on Rarefied Gas Dynamics*, American Institute of Physics, vol. 762, Melville, NY: AIP Conference Proceedings, 2005, pp. 719–724.

[18] S. Loyalka, "Thermal transpiration in a cylindrical tube," *Physics of Fluids*, vol. 12, no. 11, pp. 2301–2305, 1969.

[19] E. H. Kennard, *Kinetic Theory of Gases With an Introduction to Statistical Mechanics*. McGraw-Hill, 1938.

[20] F. M. White, *Fluid Mechanics*, 5th ed. New York: McGraw-Hill, 2003.

[21] S. Zhang and D. B. Bogy, "A heat transfer model for thermal fluctuations in a thin slider/disk air bearing," *International Journal of Heat and Mass Transfer*, vol. 42, pp. 1791–1800, 1999.

[22] D. Chen, N. Liu, and D. Bogy, "A phenomenological heat transfer model for the molecular gas lubrication system in hard disk drives," *Journal of Applied Physics*, vol. 105, p. 084 303, 2009.

[23] Y. Hu, "Head-Disk-Suspension Dynamics," PhD thesis, University of California, Berkeley, 1996.

[24] S. Lu, "Numerical Simulation of Slider Air Bearings," PhD thesis, University of California, Berkeley, 1997.

[25] B. Cox and D. B. Bogy, *The CML Air Bearing Design Program (CMLAir), Version 7 User Manual*, 2007.

[26] J. Greenwood and J. Williamson, "Contact of nominally flat surfaces," *Proceedings of the Royal Society of London*, vol. 295, 300319, 1966.

[27] D. Chen and D. B. Bogy, "Intermolecular force and surface roughness models for air bearing simulations for sub-5 nm flying height sliders," *Microsystem Technologies*, vol. 13, pp. 1211–1217, 2007.

[28] P. Bhargava, "Numerical Simulations of the Head-Disk Interface in Hard Disk Drives," PhD thesis, University of California, Berkeley, 2008.

[29] L. Wu and D. B. Bogy, "Effect of the Intermolecular Forces on the Flying Attitude of Sub-5 NM Flying Height Air Bearing Sliders in Hard Disk Drives," *Journal of Tribology*, vol. 124, no. 3, pp. 562–567, 2002.

[30] V. Gupta and D. B. Bogy, "Dynamics of sub-5-nm air-bearing sliders in the presence of electrostatic and intermolecular forces at the head-disk interface," *IEEE Transactions on Magnetics*, vol. 41, no. 2, 2005.

[31] J. Zheng and D. B. Bogy, *CML TFC Code User's Manual*, 2009.

[32] W. M. Kays and M. E. Crawford, *Convective Heat and Mass Transfer*. New York: McGraw-Hill, 1993.

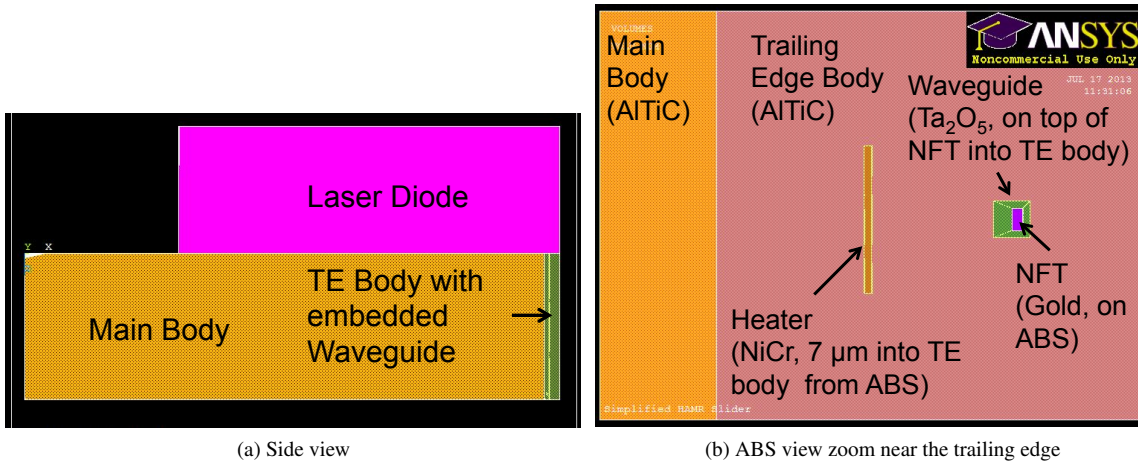(a) Side view

(b) ABS view zoom near the trailing edge

Figure 1: The simplified HAMR slider finite element model. The trailing edge (TE) body contains the embedded waveguide and near field transducer (NFT). The bottom of the NFT is on the air bearing surface (ABS). The heater is embedded into the TE body 7 μm from the ABS. The laser diode is attached to the back of the slider, opposite the ABS.
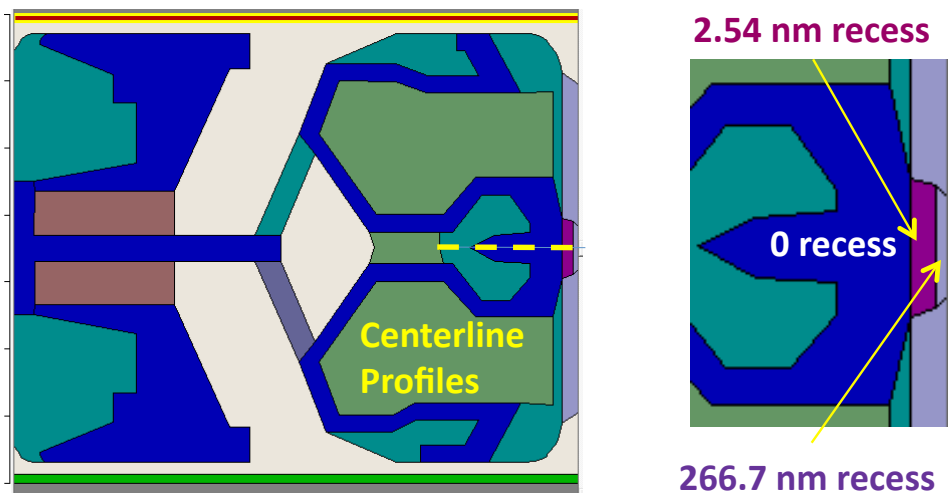

Figure 2: ABS rail design used in the air bearing solver. The colors reflect different etch depths. The base etch depth (deepest recess) of the ABS design is 1.651 μm. The yellow dashed line in the left image indicates the location of centerline profiles shown in upcoming sections. The center of the trailing edge is shown in detail in the right image. The trailing edge region contains the NFT.
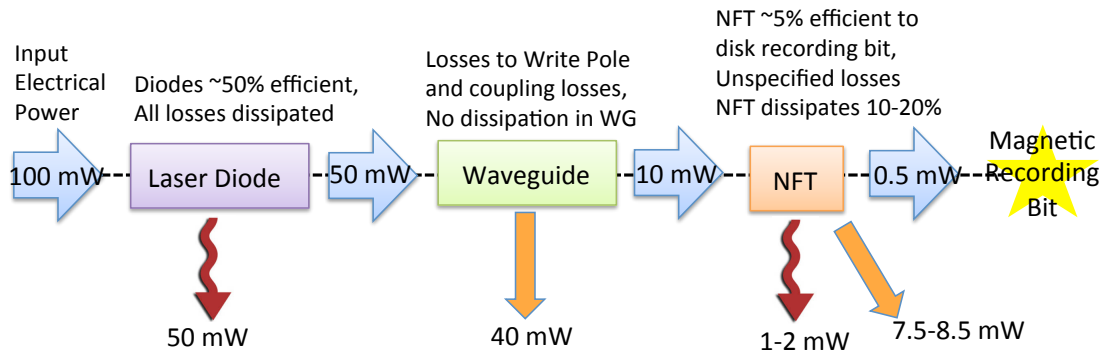
Figure 3: The power budget assumed for this study based on several sources [3, 8, 9, 14, 15]. Power absorbed by the laser diode and NFT is assumed to be dissipated as heat (red wiggle arrows). All other unspecified losses (orange straight arrows) are ignored in the thermo-mechanical modeling.
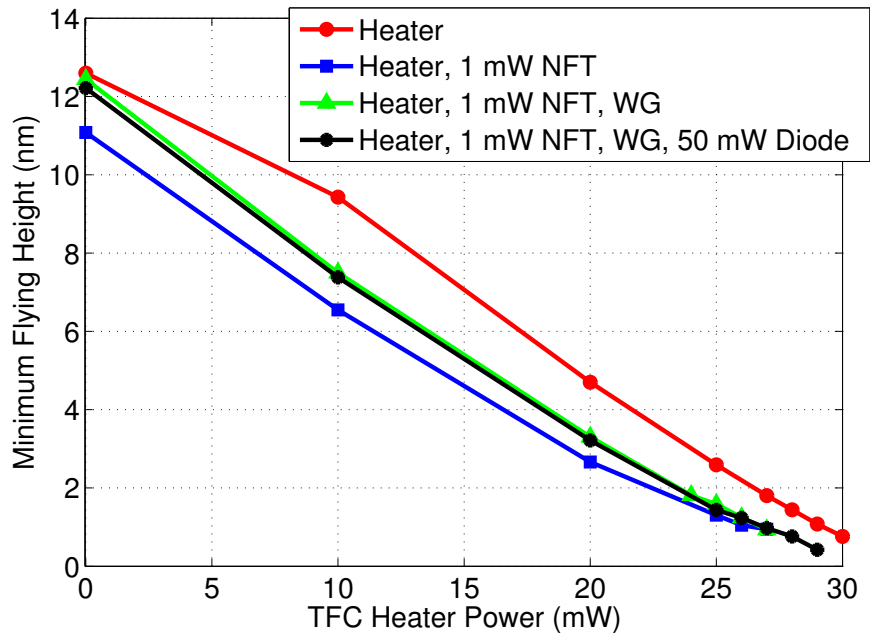
Figure 4: Slider Component Study – Minimum Flying Height: Minimum flying height for different slider types. WG indicates the presence of the waveguide. If present, the NFT heat generation rate is 1 mW, and the laser diode dissipates 50 mW.
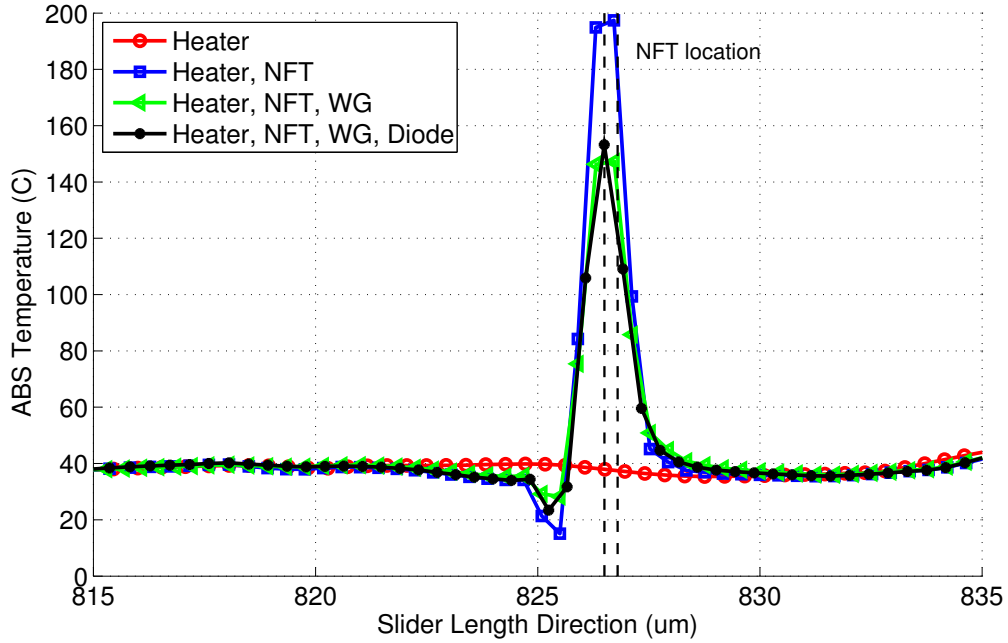
(a) ABS temperature for the case of 27-mW heater power
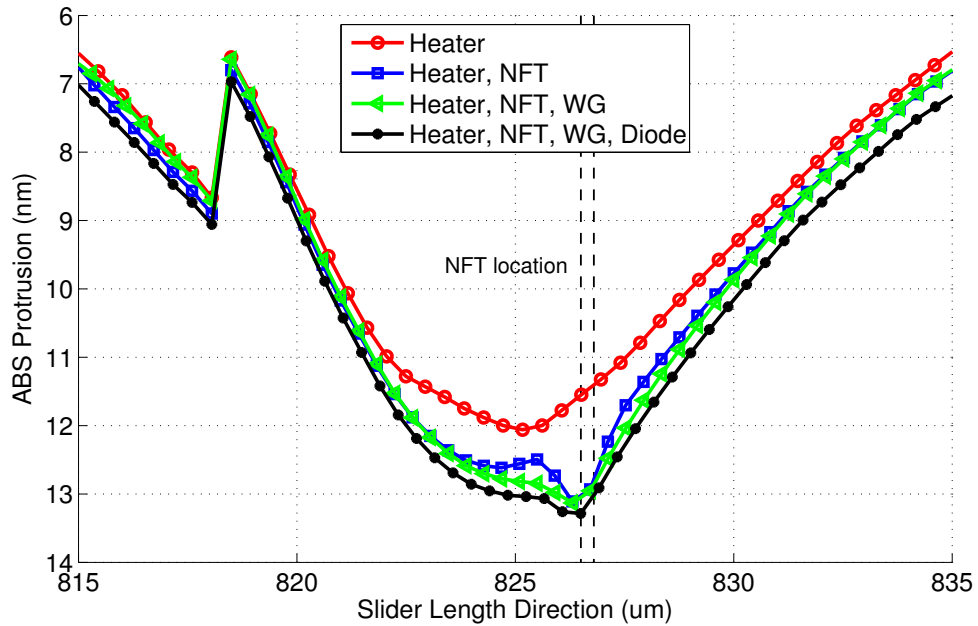
(b) ABS protrusion for the case of 27-mW heater power

Figure 5: Slider Component Study – ABS Temperature and Protrusion: Centerline profiles for (a) ABS temperature and (b) ABS thermal protrusion near the trailing edge for sliders with varying amount of components. For all cases, the heater power is 27 mW. If present, the NFT heat generation rate is 1 mW, and the laser diode dissipates 50 mW. The abrupt changes in ABS protrusion are due to the rail design.
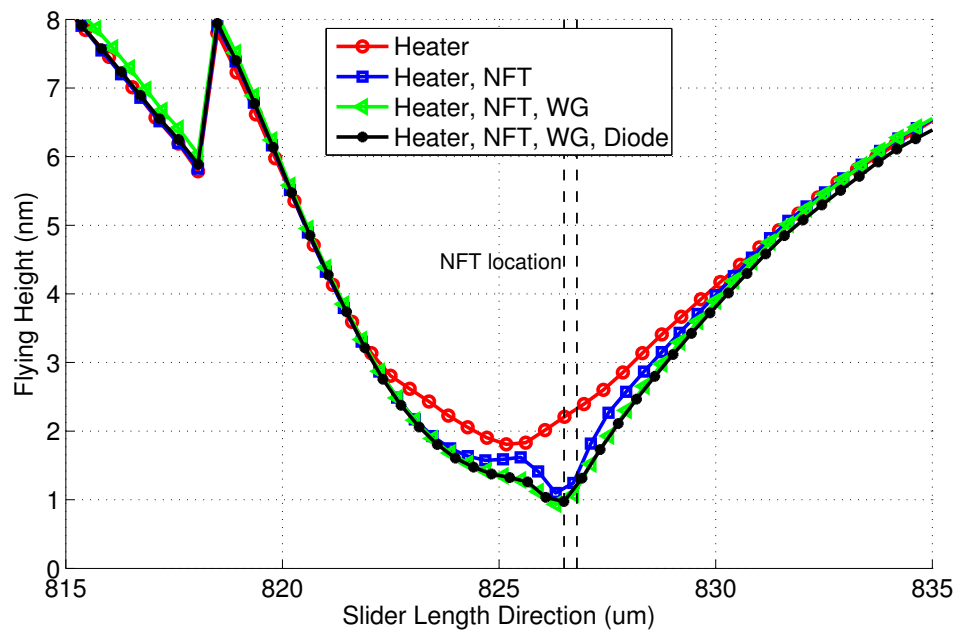
Figure 6: Slider Component Study – Flying Height: Flying height centerline profile near the trailing edge for the case of 27-mW heater power, 1-mW NFT heat generation rate, and 50-mW diode dissipation rate.
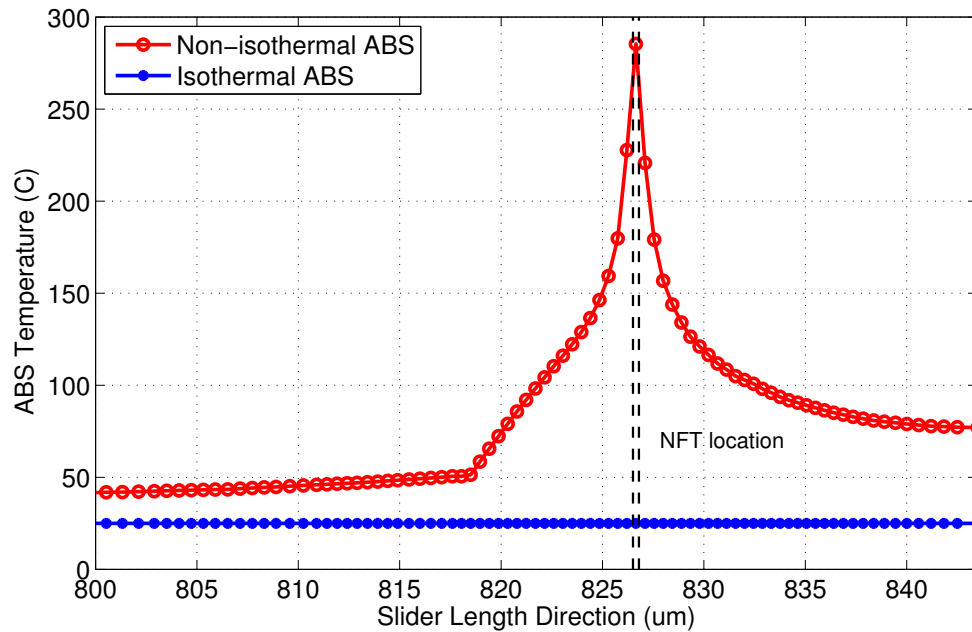
(a) ABS temperature centerline profiles
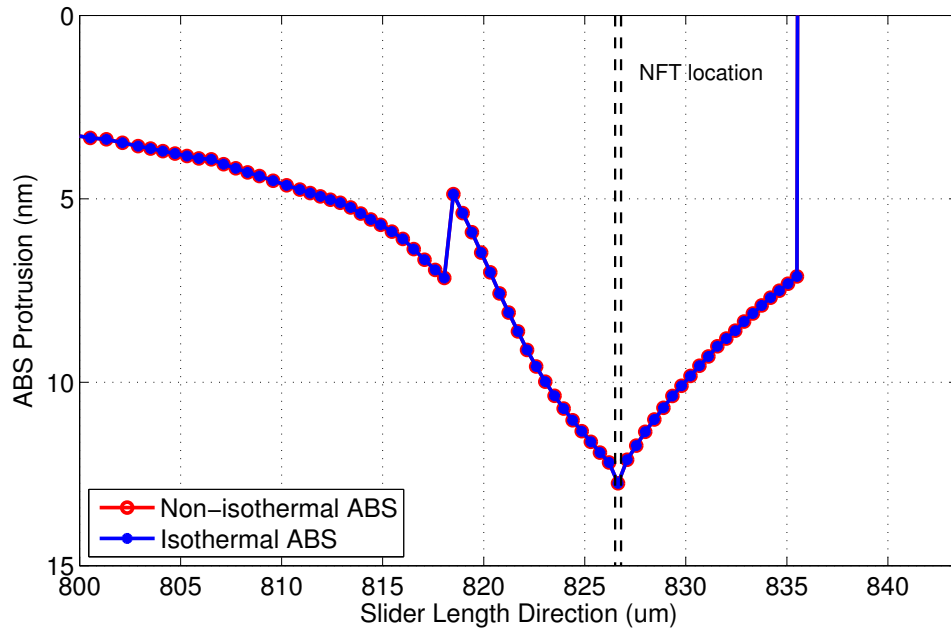
(b) ABS protrusion centerline profile for both cases

Figure 7: Air Bearing Solver Governing Equation Study: (a) ABS temperature and (b) thermal protrusion near the trailing edge used as boundary conditions for the air bearing solver. By specifying the ABS temperature to be ambient temperature (isothermal ABS case), the air bearing solver governing equation reduces to the isothermal molecular gas lubrication equation (Equation 3). By allowing for lateral variation in the ABS temperature due to heat-dissipating NFT and TFC heater elements (non-isothermal ABS case), the air bearing solver governing equation remains the fully generalized molecular gas lubrication equation (Equation 1). The thermal spot due to the NFT has a maximum temperature of $285°C$ and is approximately 3.6 μm FWHM. The abrupt changes in ABS protrusion are due to the rail design.
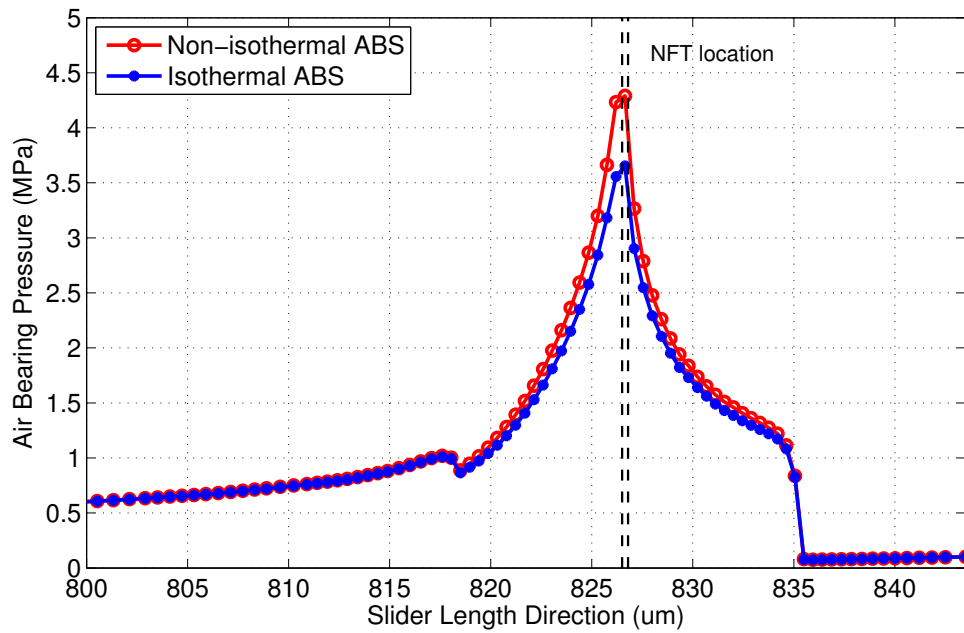
(a) Air bearing pressure near trailing edge
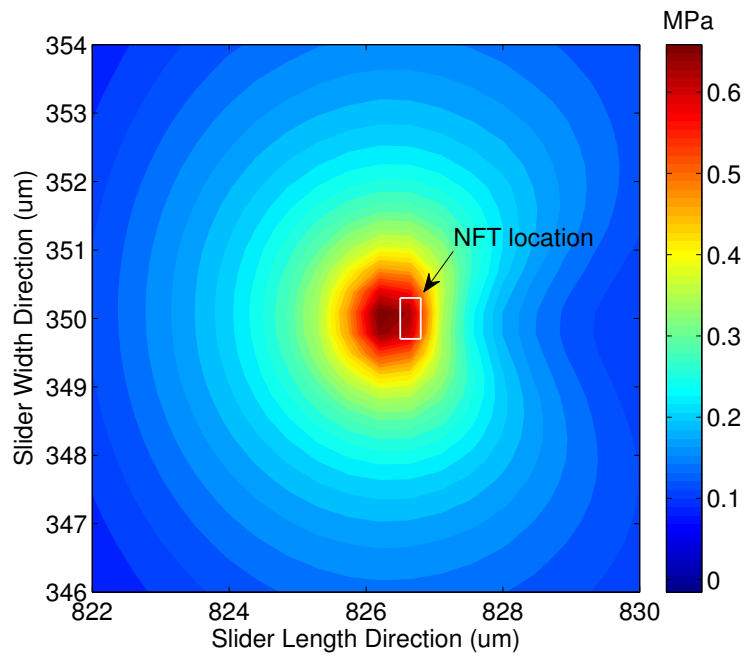
(b) Difference in air bearing pressure (non-isothermal case minus isothermal case) near the NFT

Figure 8: Air Bearing Solver Governing Equation Study – Effect on Air Bearing Pressure
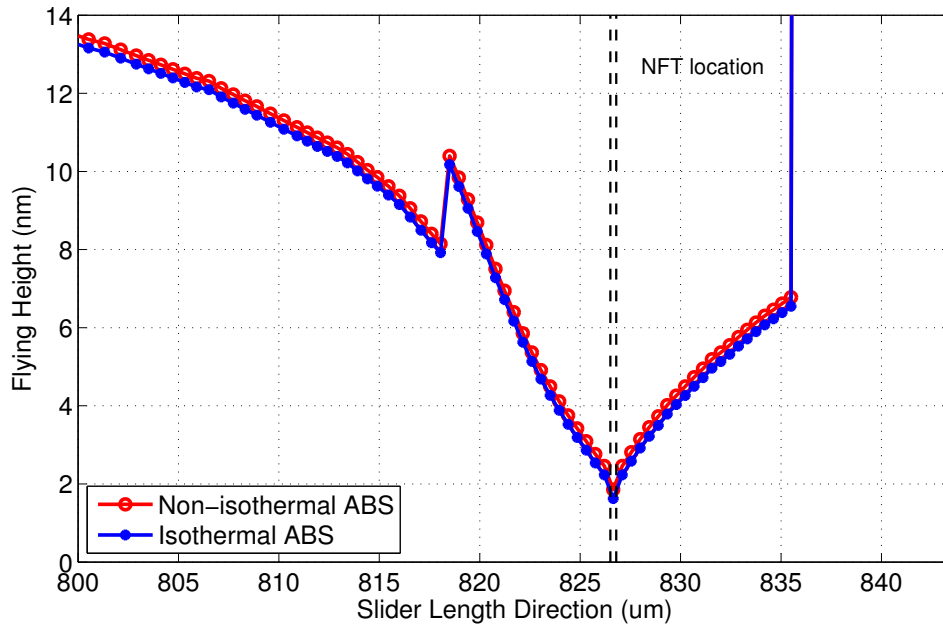
(a) Flying height centerline profile near the trailing edge
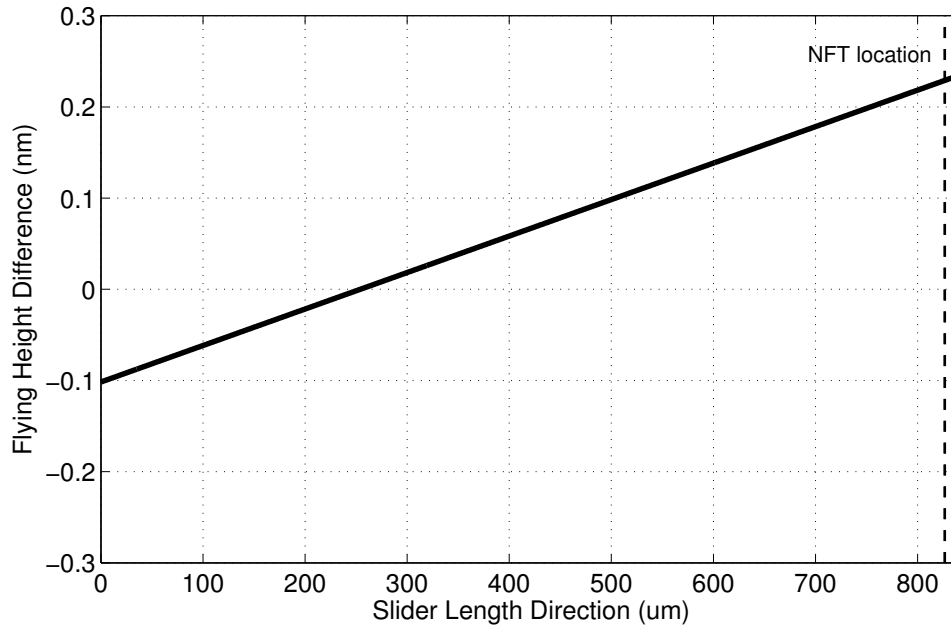
(b) Flying height difference (non-isothermal case minus isothermal case) along the slider's length at the centerline

Figure 9: Air Bearing Solver Governing Equation Study – Effect on Flying Height
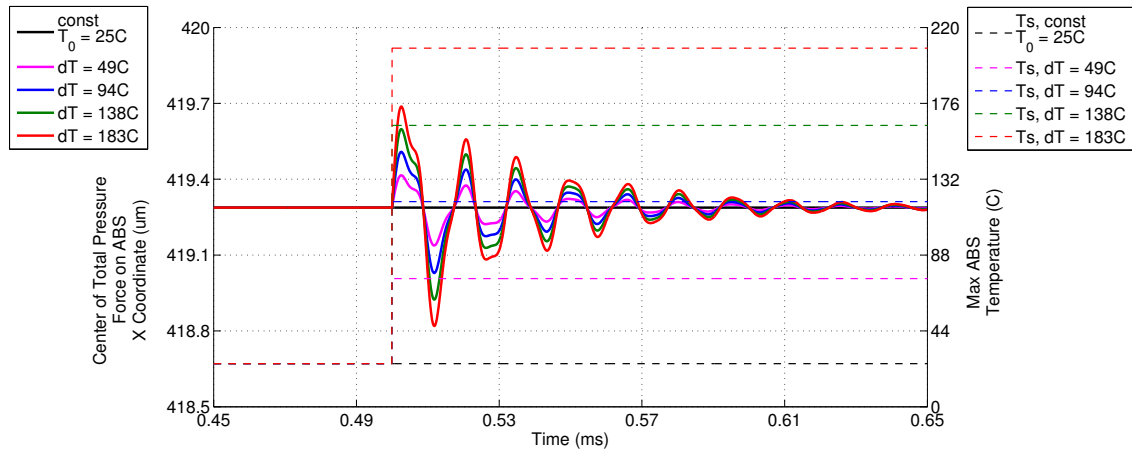
(a) Step response: center of pressure *x* coordinate
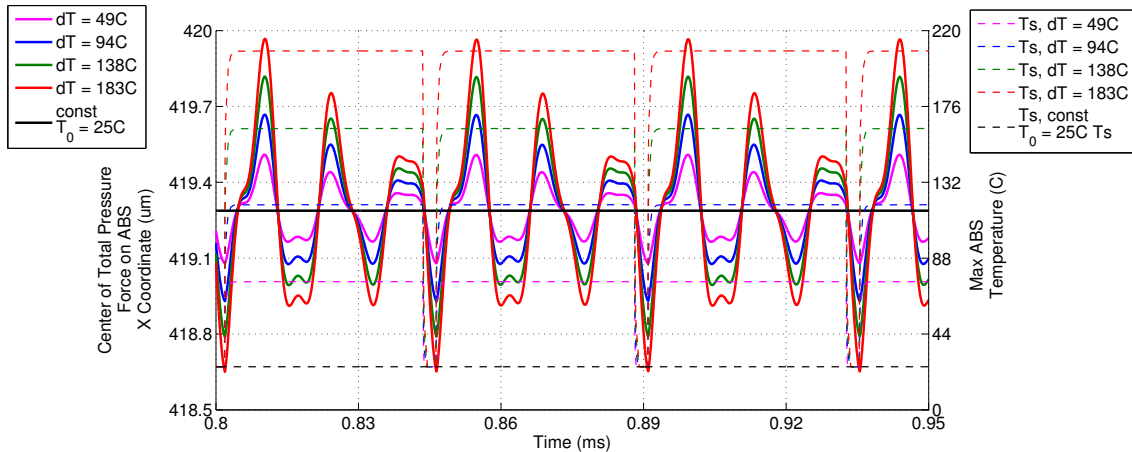
(b) Pulsed response: center of pressure *x* coordinate

Figure 10: Dynamic Solver Results – *x* Coordinate: Time history of the center of pressure *x* coordinate (slider length direction coordinate) for the total integrated pressure acting on the ABS. The responses to (a) a step response to a suddenly applied ABS temperature distribution and (b) a pulsed ABS temperature profile are shown. The center of pressure *x* coordinate is plotted with solid lines (left axis) and the maximum ABS temperature is plotted with dashed lines (right axis). The total pressure force acting on the ABS is the sum of the air bearing force (~ 2.504 g-force) and intermolecular forces (~ -0.004 g-force). There is no contact.
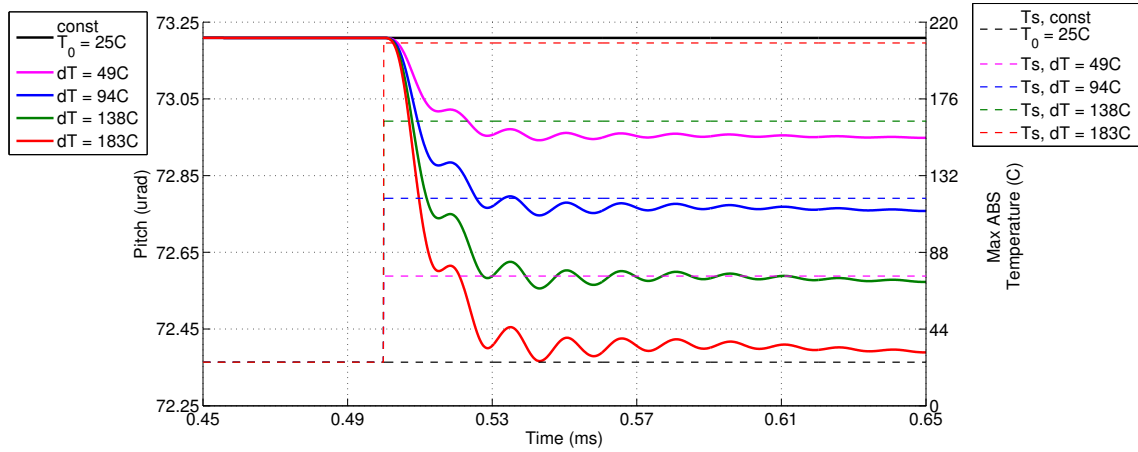
(a) Step response: pitch angle
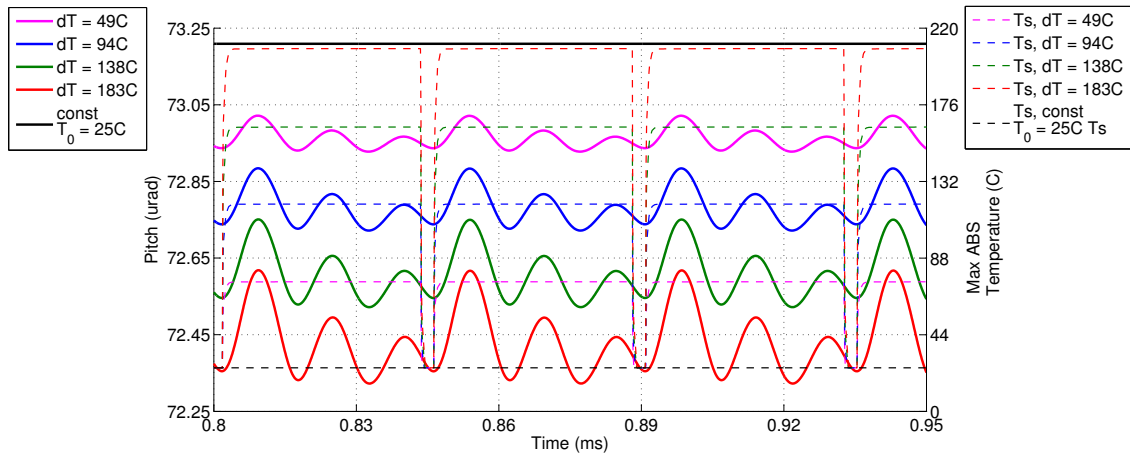
(b) Pulsed response: pitch angle

Figure 11: Dynamic Solver Results – Pitch: Time history of the slider's pitch angle in response to (a) a step response to a suddenly applied ABS temperature distribution and (b) a pulsed ABS temperature profile. The slider pitch angle is plotted with solid lines (left axis) and the maximum ABS temperature is plotted with dashed lines (right axis).
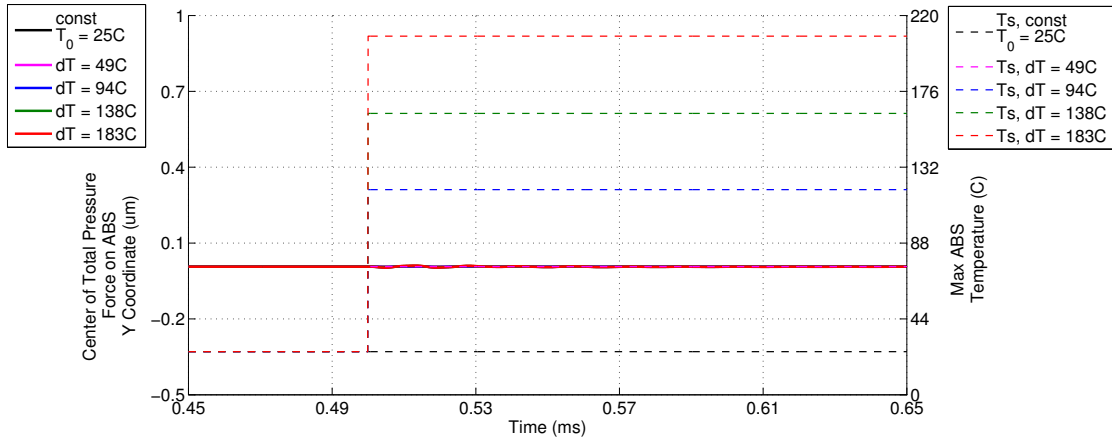
(a) Step response: center of pressure *y* coordinate
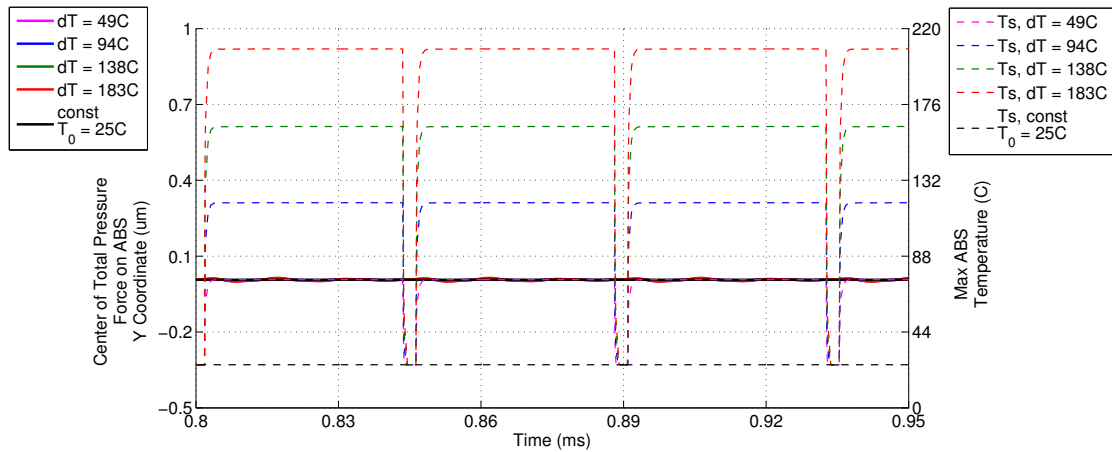
(b) Pulsed response: center of pressure *y* coordinate

Figure 12: Dynamic Solver Results – *y* Coordinate: Time history of the center of pressure *y* coordinate (slider width direction coordinate) for the total integrated pressure acting on the ABS. The responses to (a) a step response to a suddenly applied ABS temperature distribution and (b) a pulsed ABS temperature profile are shown. The center of pressure *y* coordinate is plotted with solid lines (left axis) and the maximum ABS temperature is plotted with dashed lines (right axis). The total pressure force acting on the ABS is the sum of the air bearing force (~ 2.504 g-force) and intermolecular forces (~ -0.004 g-force). There is no contact.
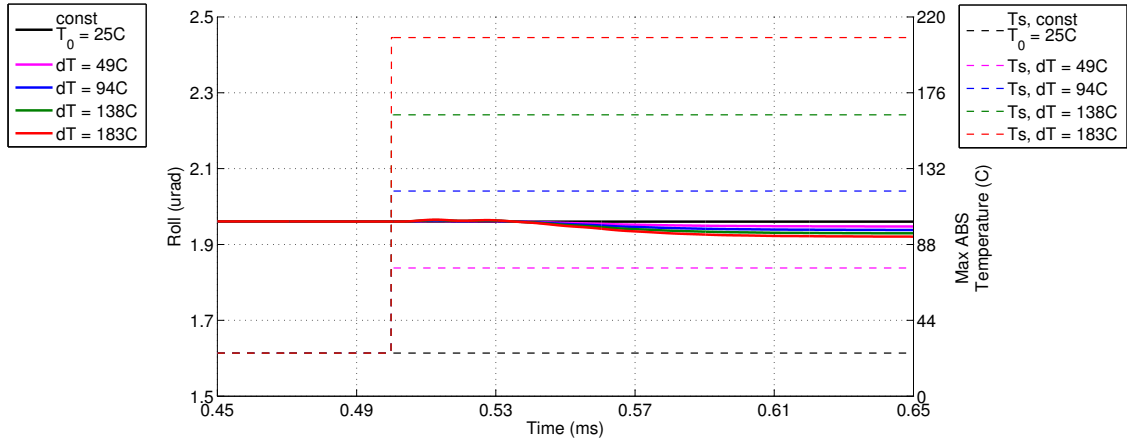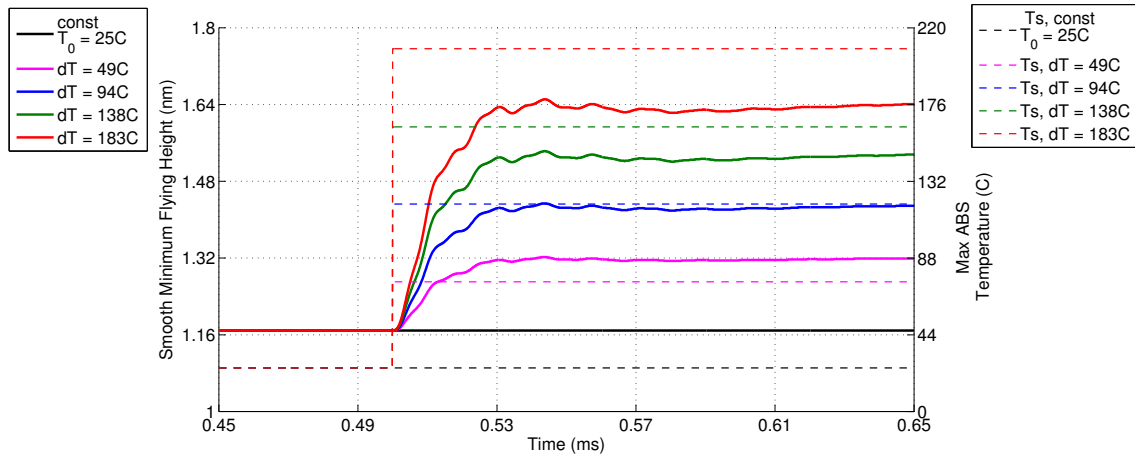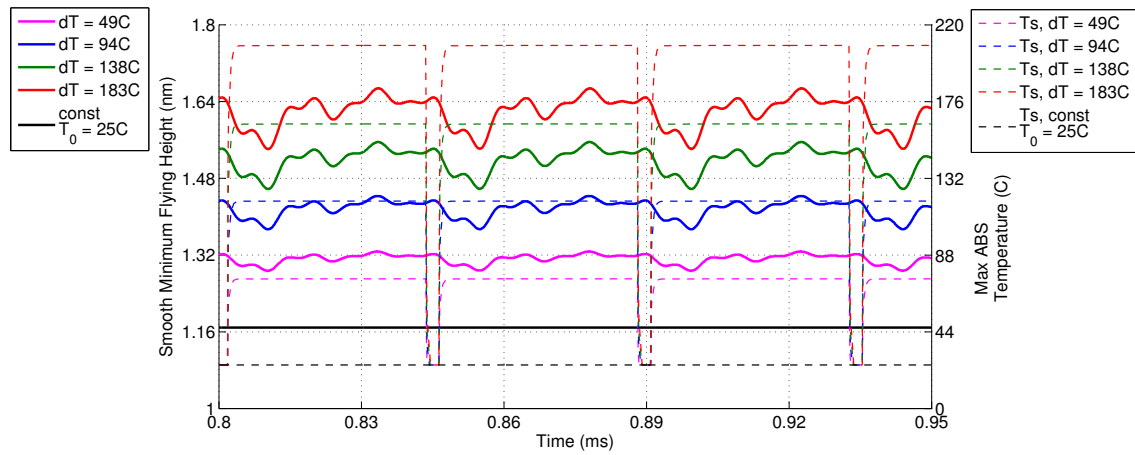
(a) Step response: roll angle
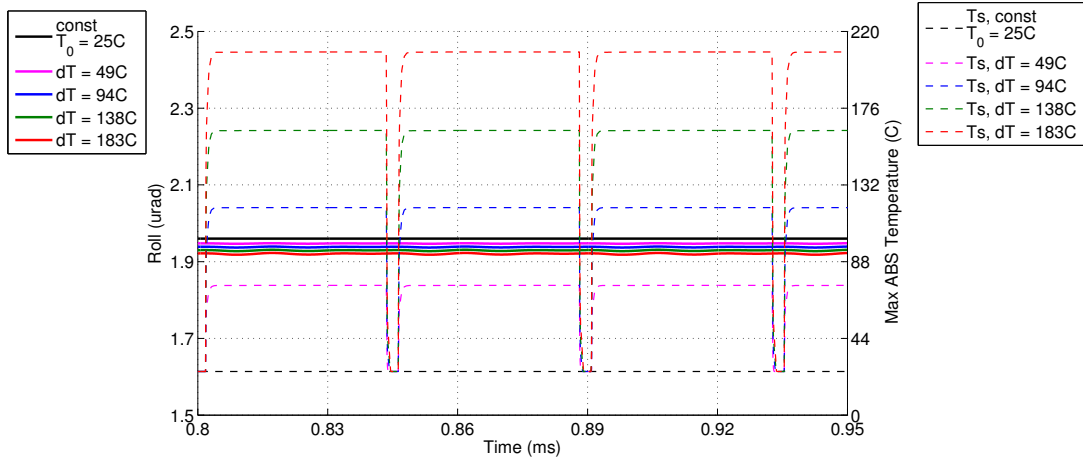
(b) Pulsed response: pitch angle

Figure 13: Dynamic Solver Results – Roll: Time history of the slider's roll angle in response to (a) a step response to a suddenly applied ABS temperature distribution and (b) a pulsed ABS temperature profile. The slider roll angle is plotted with solid lines (left axis) and the maximum ABS temperature is plotted with dashed lines (right axis).

(a) Step response: minimum flying height

(b) Pulsed response: minimum flying height

Figure 14: Dynamic Solver Results – Minimum Flying Height: Time history of the slider's minimum flying height in response to (a) a step response to a suddenly applied ABS temperature distribution and (b) a pulsed ABS temperature profile. The minimum flying height is plotted with solid lines (left axis) and the maximum ABS temperature is plotted with dashed lines (right axis).